NANO LETTERS

pubs.acs.org/NanoLett
Letter

Atomic-Scale Optical Microscopy with Continuous-Wave Mid-Infrared Radiation

Felix Schiegl,[#] Valentin Bergbauer,[#] Svenja Nerreter, Valentin Giessibl, Fabian Sandner, Franz J. Giessibl, Yaroslav. A. Gerasimenko, Thomas Siday,* Markus A. Huber,* and Rupert Huber

Cite This: *Nano Lett.* 2026, 26, 1689−1696

ABSTRACT: Understanding matter at the most fundamental level requires optical microscopy with ever-higher spatial resolution. Scanning near-field optical microscopy (SNOM) has enabled important advances, circumventing the diffraction limit of light by confining it to the apex of a sharp metallic tip. However, the mesoscopic tip geometry restricts the spatial resolution to the nanometer scale. Here, using a conventional tabletop continuous-wave mid-infrared laser and intensity-based detection we observe optical signals modulated on Ångstrom length scales, consistent with light emission from atomically confined tunneling currents. The emergence of near-field optical tunneling emission (NOTE) — considered a strong-field excitation process — under continuous-wave driving is remarkable, as it typically requires ultrashort high-intensity laser pulses. Further, we find that anharmonic tip oscillation can influence the signal and propose strategies to mitigate this effect. Our findings enable the use of this tunneling-mediated contrast mechanism with standard optical setups, establishing a pathway to optical imaging with unprecedented resolution.

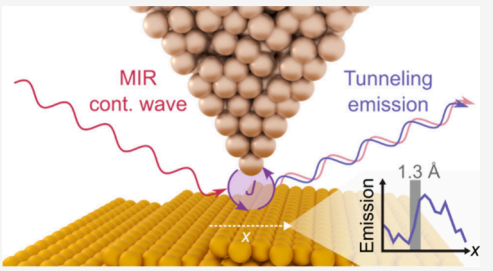

KEYWORDS: *near-field microscopy, optical microscopy, nanoscopy, mid-infrared, near-field optical tunneling emission (NOTE)*

To deepen our understanding of matter at its most fundamental level, advancing optical microscopy to the shortest possible length scales is crucial. While super-resolution techniques have successfully overcome the diffraction limit of light,[1] they typically rely on fluorescent labeling and are therefore often incompatible with solid-state systems. An alternative pathway has been the use of plasmonic nanostructures, where extreme confinement of optical fields in picocavities has enabled single-molecule spectroscopy.[2] However, this approach remains restricted, as it cannot be applied effectively at spectral ranges far from plasmonic resonances and is usually unsuitable for imaging applications. Near-field optical microscopy (SNOM) has proven to be a universal method of optical imaging beyond the diffraction limit, where sharp metallic tips act as antennas that confine light in an ultrabroad frequency range.[3,4] Despite its versatility[5−14] the spatial resolution of SNOM has so far been limited to roughly ten nanometers.[4] Recent progress, enabled by nanometer-scale tip oscillation amplitudes using self-sensing quartz sensors (e.g. qPlus[15]) in ultrahigh vacuum, has demonstrated a resolution improvement down to the single-nanometer scale in the visible spectral range using plasmonic tips.[16]

Achieving true atomic resolution, however, requires a fundamentally different contrast mechanism, in which the carrier wave of light drives atomically confined tunneling currents between the tip and the sample. By electrically detecting the rectified component of these currents, lightwave-driven scanning tunneling microscopy has enabled insights into ultrafast atomic-scale dynamics.[17−20] Recently, we have developed a more direct way to read out these a.c. tunneling currents by detecting the light emitted from them, thereby enabling all-optical microscopy with atomic-scale spatial resolution (Figure 1a).[21] Reaching the strong-field regime where the carrier wave of light can coherently drive electrons — enabling lightwave electronics[22] — has so far only been possible with ultrafast tabletop lasers or free-electron lasers.[23] This requirement has posed a major barrier to broader adoption of this contrast mechanism within the SNOM community, where continuous-wave illumination (Figure 1b) and intensity-based detection are an established standard.[4]

Here, we demonstrate that, surprisingly, tunneling-current-mediated contrast can be accessed even with a conventional, continuous-wave mid-infrared (MIR) setup based on a tabletop quantum cascade laser and intensity-based detection, making atomic-scale optical microscopy broadly compatible with existing near-field platforms. We observe optical signals that emerge only at atomic-scale distances, in line with the near-field optical tunneling emission (NOTE) mechanism rather than conventional SNOM. We further identify potential

Received: October 23, 2025
Revised: January 14, 2026
Accepted: January 15, 2026
Published: January 22, 2026

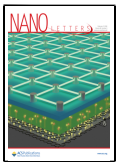

https://doi.org/10.1021/acs.nanolett.5c05319
Nano Lett. 2026, 26, 1689−1696

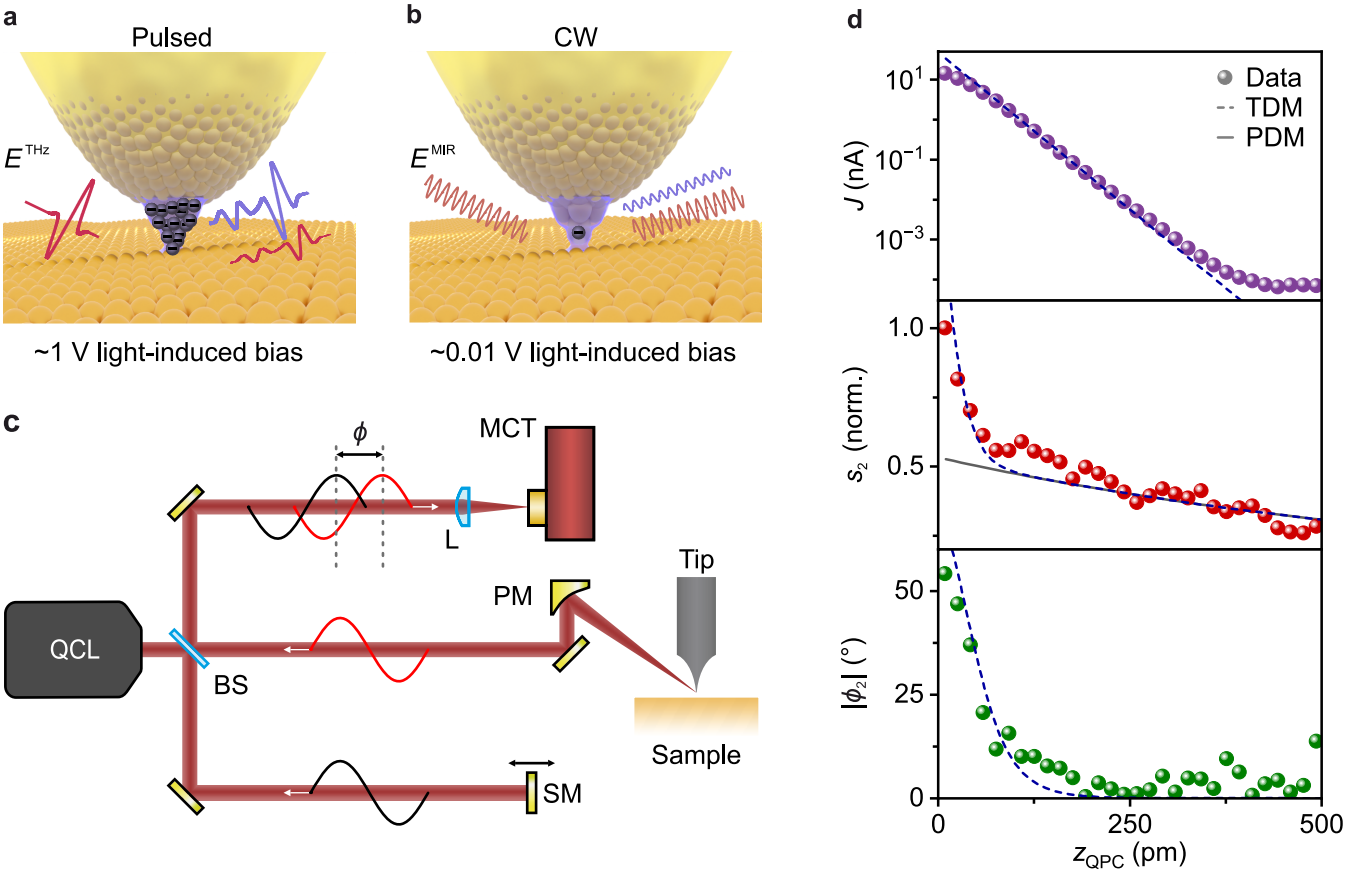

Figure 1. Near-field optical tunneling emission (NOTE) with mid-infrared (MIR) continuous-wave (cw) radiation. (a) Schematic of ultrafast terahertz (THz) NOTE microscopy. THz pulses are focused onto a sharp metallic tip placed within atomic distance to an Au(111) surface. The transient electric field induced lightwave bias on the order of 1 V drives electrons back and forth the tunneling junction, leading to a NOTE waveform (violet) being emitted alongside the conventional near-field signal (red). (b) Schematic of NOTE microscopy with cw MIR radiation, where the peak lightwave-induced bias is several orders of magnitude smaller, leading to much lower lightwave-induced tunneling currents. (c) Experimental setup: Radiation from a commercial quantum cascade laser (QCL) is focused onto a sharp metallic tip placed above an Au(111) sample using a parabolic mirror (PM). The backscattered light is collimated and, via a beamsplitter (BS), superimposed with a split-off portion of the beam that is harmonically modulated in its phase ϕ using a piezo-driven shaker mirror (SM). Using this pseudoheterodyne detection scheme, the amplitude and phase of the scattered light detected with a mercury-cadmium-telluride photodiode (MCT) can be extracted (see Supporting Information Section 2). (d) Signals originating from the tip-sample junction as a function of the tip-sample distance z_{QPC} at the point of closest approach (oscillation amplitude A = 200 pm), calibrated via the expected value for the tunneling current J at the quantum point contact (QPC). Top panel: tunneling current J (d.c. bias voltage V_{dc} = 3 mV). Central and bottom panel: simultaneously acquired near-field amplitude s_2 (red) and magnitude of the relative phase $|\phi_2|$ (green), demodulated at the second harmonic of the tip oscillation frequency. The dashed lines correspond to fits using the tunneling dipole model (TDM, see Figure 2), while the solid line shows the contribution of only the point dipole model (PDM).

artifacts that can arise under these unique experimental conditions and implement strategies to exclude their influence on the observed features. Our findings open the door to atomic-scale imaging using tools that are already established in the near-field community, offering a practical route to optical access on the level of individual atoms.

We use a well-established optical setup for near-field microscopy based on a commercial quantum cascade laser combined with pseudoheterodyne detection[24] and couple it to a commercial scanning probe microscope (see Figure 1c and Supporting Information, Sections 1 and 2). By mounting our tips to stiff qPlus sensors (ref 15, Supporting Information Section 3), we achieve precise control over the tip motion, allowing for reduction of the oscillation amplitude by several orders of magnitude: from the ∼10−100 nm range typical of conventional cantilever-based SNOM, to 100 pm. Additionally, frequency-modulation noncontact atomic force microscopy (AFM) enables us to stabilize the tip-sample separation with atomic-scale precision. Moreover, our experimental configuration provides simultaneous access to the scattered optical fields and the rectified tunneling currents between tip and sample, allowing for distinction of effects based on tunneling and conventional near-field scattering.

First, the dependence of the scattered optical signal on the tip-sample distance z is explored. To this end, we approach an Au(111) surface (oscillation amplitude A = 200 pm, d.c. bias voltage V_{dc} = 3 mV) while simultaneously recording the tunneling current J, the near-field amplitude s_2, and the magnitude of the relative optical phase of the scattered light $|\phi_2|$ (see Figure 1d). To calibrate the absolute tip-sample distance z_{QPC} at the point of closest approach during the oscillation cycle of the tip, the exponentially decaying tunneling current is extrapolated to the value expected in quantum point contact (QPC, Supporting Information Section 4).[25] The measured near-field amplitude s_2 and the magnitude of the phase $|\phi_2|$ are shown in the central and bottom panel of Figure 1d. At tip-sample distances larger than z_{QPC} = 150 pm, the observed behavior aligns well with what is expected for a

https://doi.org/10.1021/acs.nanolett.5c05319
Nano Lett. 2026, 26, 1689−1696

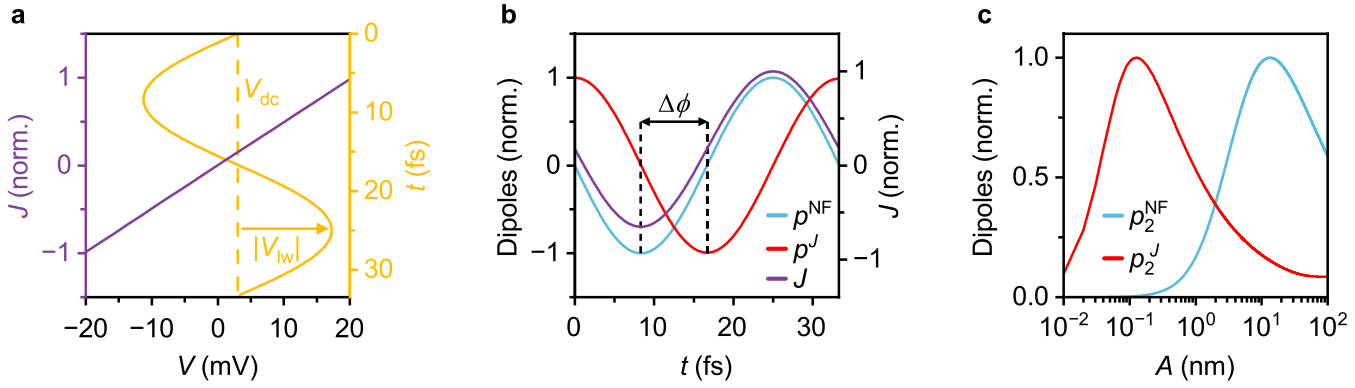

Figure 2. Tunneling dipole model (TDM) of the MIR cw NOTE signal. (a) Modeling the time-dependent tunneling currents. The mid-infrared radiation acts as a time-dependent bias voltage $V_{lw}(t)$ that adds to the applied d.c. voltage (V_{dc} = 3 mV, dashed yellow line). The total bias $V(t) = V_{dc} + V_{lw}(t)$ (yellow line) drives a time-dependent tunneling current J according to the conductance of the gold substrate (violet). (b) Temporal evolution of the near-field dipole p^{NF} and tunneling dipole p^J during one oscillation cycle of the driving field simulated with the TDM. p^J (red) is formed as a time integral over the tunneling current J (violet), resulting in a phase shift $\Delta\phi = \pi/2$ (see vertical black dashed lines) compared to p^{NF} (blue, calculated via the point dipole model (PDM)). (c) Calculated oscillation amplitude dependence of the dipoles p_2^{NF} and p_2^J, demodulated at the second harmonic of the oscillation frequency. Picometric oscillation amplitudes (A < 1 nm) favor the contribution of p_2^J over p_2^{NF}. By extracting the sum of p_2^{NF} and p_2^J for a constant value of the oscillation amplitude A = 200 pm while varying the average tip-sample separation, we reproduce the experimentally observed decay of the optical signals as well as the emerging phase shift (dashed lines in Figure 1d). Simultaneously, the modeled tunneling current J also matches the experimental data.

conventional SNOM signal: s_2 increases gradually with decreasing z_{QPC}, and $|\phi_2|$ remains constant within the noise floor of the detection. Intriguingly, at distances below 100 pm, s_2 rises much more steeply, accompanied by a distinct phase shift of ∼50°. This distance dependence of the optical signals cannot be reproduced by the established point dipole model (PDM[26]), which predicts no pronounced phase shift and a smaller increase in amplitude at small tip-sample separations (Figure 1d, solid line). Instead, the observed features in s_2 and $|\phi_2|$ are consistent with light emission from a.c. tunneling currents which are driven by the electric field of light and can be described by a straightforward tunneling dipole model (TDM, Figure 1d, dashed lines; Supporting Information Section 5).

In this model, the incident light not only induces a near-field dipole p^{NF} at the apex of the tip, as in conventional SNOM models, but also acts as a transient bias $V_{lw}(t)$, that adds to the applied d.c. bias V_{dc}. For strong fields and small tip-sample separations, this drives a tunneling current based on the I-V-curve of the tip-sample system as measured with scanning tunneling spectroscopy (see Figure 2a, purple), evaluated at the time-dependent bias values $V(t) = V_{dc} + V_{lw}(t)$ (Figure 2a, yellow). As a result, the tunneling current becomes time dependent (Figure 2b, purple) and induces an additional tunneling dipole p^J through charge accumulation (Figure 2b, red). Assuming instantaneous tunneling, the lightwave-induced bias, which is proportional to p^{NF} (Figure 2b, blue), and the tunneling current are in phase. However, due to the time-integrating process of charge accumulation via tunneling, the induced tunneling dipole p^J shows a $\pi/2$ phase shift (Figure 2b).

Both time-dependent dipoles radiate into the far field, directly imprinting their relative phase shift onto the measured signals. By incorporating the exponential distance-dependence of the tunneling current, the model also captures the influence of varying tip-sample separation, thereby allowing us to incorporate the effect of the tip oscillation. Thereby, the influence of the amplitude set point A on the relative magnitude of the experimentally accessible dipoles, p_2^{NF} and p_2^J, obtained by demodulating at the second harmonic of the oscillation frequency, can be calculated (Figure 2c). While for conventional oscillation amplitudes (∼10−100 nm), the relative contribution of the tunneling-induced signal is negligibly small, operating at subnanometer amplitude set points drastically enhances the relative charge-transfer-induced signal (compare Figure 2c).

Comparing this model with the experimental data in Figure 1d, it is obvious that the TDM (dashed lines) does not only reproduce the gradual increase of the scattered optical near-field signal with decreasing distance but simultaneously also the rapid rise in signal at tip-sample separations $z_{QPC} \lesssim 150$ pm. Simultaneously, the model accurately captures the corresponding phase shift as well as the tunneling current as a sum of the d.c. current J_{dc} and the lightwave-driven current J_{lw}, confirming that the observed atomic-scale signal originates from tunneling emission. The emergence of light emission from coherent electron driving resembles the Brunel effect in atoms,[27] but here the subcycle current traverses the tip-sample junction, confining the effect to a single atomic-scale gap. This observation comes as a surprise, as strong-field effects are not usually accessible with a tabletop continuous-wave source. In Keldysh's model of tunnel ionization[28] — conceptualized for gases but commonly also applied to solids — an electron tunnels through an approximately triangular potential barrier whose width depends on the applied electric field, making tunneling processes only relevant for strong fields. In the present experiment, however, the physical situation is fundamentally different. The tunneling occurs across the vacuum gap between tip and sample,[29] whose width is primarily determined by the geometric tip-sample separation. The role of the optical field is therefore not to reshape the barrier itself but rather to induce a transient bias across an already narrow tunneling junction. This transient lightwave-induced bias modulates the energetic alignment of the tip and sample Fermi levels, thereby enabling tunneling even at moderate field strengths. Owing to the local field enhancement at the tip apex, we estimate the lightwave-induced bias to reach a few millivolts (Supporting Information Section 6). At the

https://doi.org/10.1021/acs.nanolett.5c05319
Nano Lett. 2026, 26, 1689−1696

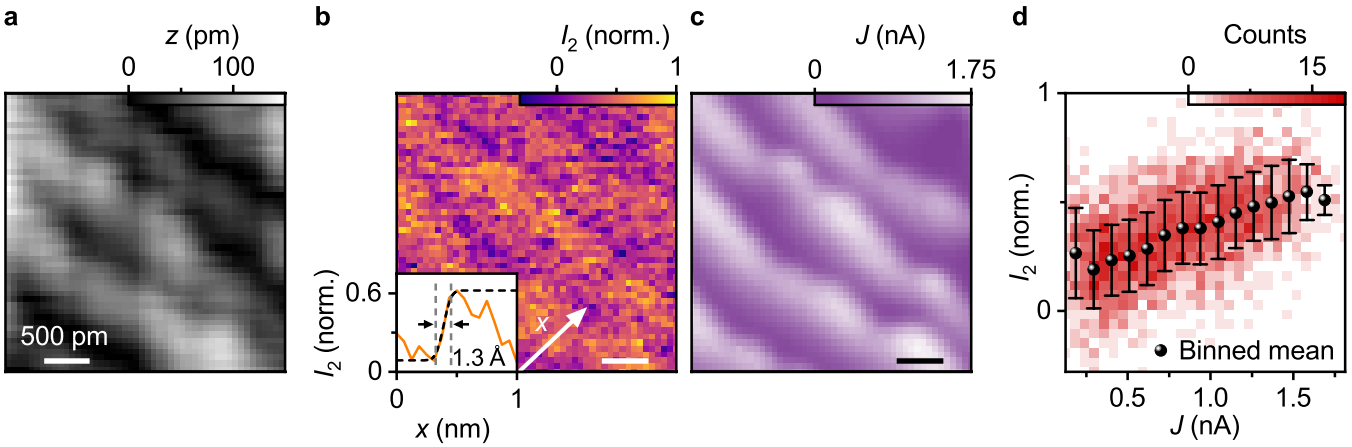

Figure 3. Optically resolving atomic-scale features using MIR cw radiation. (a) Topography of a vicinal gold surface imaged with atomic force microscopy (AFM) (oscillation amplitude A = 100 pm, frequency shift set point $\Delta\nu_{set}$ = −1.7 Hz), revealing characteristic monatomic steps. (b) Simultaneously acquired map of the scattered intensity I_2, demodulated at the second harmonic of the tip oscillation frequency. A clear contrast emerges with enhanced intensity at the atomic step edges. The inset shows a linecut of I_2 along x. Fitting a step in the signal with an error function (black dashed line), we find a spatial modulation on the length scale of 1.3 Å using a 90%−10% criterion. (c) Simultaneously acquired map of the tunneling current J, recorded under minimized d.c. bias, where a close resemblance to the I_2 map is found. (d) Two-dimensional histogram representing the pixelwise correlation between the current J and scattered intensity I_2, indicating a linear correlation between the two quantities. The color map indicates the number of pixels whose value pairs fall into each bin. The black spheres depict the data points binned exclusively along the J-axis, while the error bars represent one standard deviation. For clarity, the AFM topography was line-leveled and smoothed using a Gaussian filter.

closest tip-sample distance of z_{QPC} = 9 pm, our model predicts that on average one electron tunnels across the junction in 100 optical cycles. In the experiment, the optical excitation power (5 mW) lies within the upper range reported to be compatible with a stable tip-sample junction in low-temperature tip-based measurements,[30] and we likewise find that further increases in power lead to reduced stability, thereby constraining the achievable lightwave-induced bias. As a consequence, extremely small tip-sample distances ($z_{QPC} \lesssim 50$ pm in this experiment) are necessary to achieve sufficiently strong lightwave-driven tunneling currents for the near-field optical tunneling emission to dominate the scattering response. Yet, it shows that atomic-scale tunneling can be accessed with standard continuous-wave optical setups, paving the way toward more widespread use of tunneling-current-mediated optical contrast mechanisms.

Having used the phase shift in the optical response to confirm tunneling emission as the dominant contrast mechanism at small tip-sample distances and oscillation amplitudes, the signal quality can be improved by switching from pseudoheterodyne to intensity-based detection, sometimes also referred to as self-homodyne detection.[16] At the small amplitude set points used in this study (A < 1 nm), we find that the measured intensities I_2 demodulated at the second harmonic of the oscillation frequency are virtually background-free (Supporting Information Section 7). Moreover, the improved stability of the signal due to the simpler setup results in enhanced long-term stability. This allows us to decrease the oscillation amplitude by a factor of 2 to only 100 pm, further enhancing the tunneling emission contribution.

As this signal stems from atomically confined tunneling currents, it should also feature atomic-scale lateral resolution. To test this, we perform a 3 nm by 3 nm scan on a vicinal gold surface[31] in AFM feedback (oscillation amplitude A = 100 pm, frequency shift set point $\Delta\nu_{set}$ = −1.7 Hz). The topography (Figure 3a) clearly shows the characteristic terrace-like structure consisting of periodically spaced monatomic steps, which are known to affect the surface electronic structure of the material.[32] The simultaneously recorded scattered intensity I_2 exhibits a modulation on the same lateral scale (see Figure 3b). In particular, I_2 displays enhanced intensity at the atomic step edges. To quantitatively assess the spatial confinement of the optical signal, we extract a line profile from the two-dimensional I_2 map and analyze a representative edge feature (line profile in Figure 3b, inset). By fitting the edge with an error function, we determine the lateral distance between the 90% and 10% intensity level of the step edge, revealing a modulation on the length scale of 128 pm. As a consistency check, we analyze eight additional step edges, yielding a mean modulation width of 130 pm and a standard deviation of 35 pm (Supporting Information Section 8). Remarkably, the spatial distribution of the simultaneously measured tunneling current J for minimized d.c. bias (Figure 3c) closely mirrors that of I_2, exhibiting the same stripe-like modulation and enhanced signal at the descending edges of atomic steps. This strong similarity between I_2 and J provides further compelling evidence that the scattered light originates from tunneling electrons.

A pixel-by-pixel correlation analysis between I_2 and J (Figure 3d) reveals a clear correlation, with higher values of scattered intensity consistently associated with regions of increased tunneling current. Binning the data along the J-axis and computing the mean of I_2 for each bin (Figure 3d, black spheres) reveals an approximately linear dependence of I_2 on J. This correlation further confirms that both signals originate from the same picometric contrast mechanism, likely a modulation of the local tunneling probability, even though a partial influence of the sample's modulated topography due to small variations in tip-sample distance during scanning cannot be completely ruled out within the sensitivity of our measurement. Generally, however, we find a clear correlation between the optical signal and the tunneling currents that are conventionally used to resolve molecules and single adatoms,

https://doi.org/10.1021/acs.nanolett.5c05319
Nano Lett. 2026, 26, 1689−1696

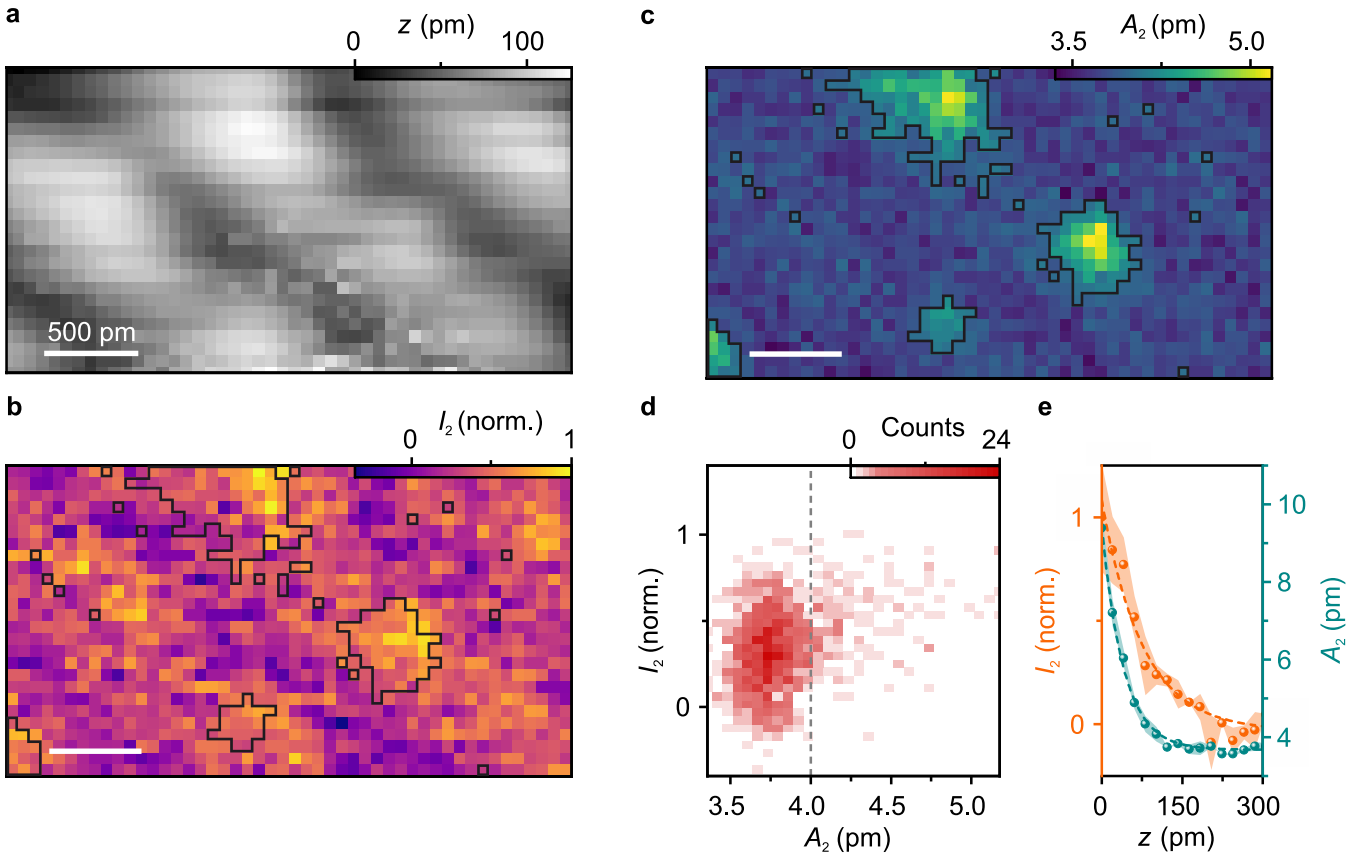

Figure 4. Optical imaging at the mechanical limit. (a) Topography of the vicinal gold surface, measured in AFM feedback mode (A = 100 pm, $\Delta\nu_{set}$ = −1.8 Hz). (b) Simultaneously recorded scattered intensity I_2, where a clear modulation can be seen. (c) Simultaneously acquired map of the mechanical tip oscillation amplitude A_2, demodulated at the second harmonic of the oscillation frequency. The scan shows local peaks of A_2, indicating anharmonicity of the tip oscillation. (d) Two-dimensional histogram representing the pixelwise correlation between I_2 and A_2, where the color map indicates the number of value pairs that fall into each bin. High values of A_2 tend to coincide with high values of I_2. The highlighted areas in b and c show the data points to the right of the gray dashed line, where A_2 > 4 pm. (e) Comparison of the distance dependence of the intensity I_2 and the second harmonic oscillation amplitude A_2, revealing different decay lengths for both signals. The dashed lines show exponential fits of the data. The experimental data in panels d and e were averaged over the forward and backward direction of the scan with the shaded area representing one standard deviation.

suggesting that our all-optical method could perform equally well.

Having reduced the oscillation amplitude to 100 pm and changed the detection scheme to enhance the signal, the signal could potentially be further increased by optimizing the tip-sample distance for the reduced oscillation amplitude. Therefore, we perform another two-dimensional scan with a frequency shift set point of −1.8 Hz, effectively approaching the tip further to the sample. The AFM topography (Figure 4a) and the scattered intensity I_2 (Figure 4b) show an overall similar behavior to the previous scan. However, apart from the previously observed variation along the step edges, I_2 displays additional hotspots of elevated intensity. To find the origin of this locally confined signal enhancement, we trace the oscillation of our scanning probe sensor by measuring the voltage signal generated by the piezoelectric quartz sensor, on which the tip is mounted. Directly accessing this signal at the second harmonic of the tip oscillation frequency A_2 via lock-in detection (Figure 4c, see Supporting Information Section 9 for the exact calibration procedure), we find that I_2 and A_2 show the same hotspots (Figure 4b and 4c). This suggests that the hotspots in I_2 are linked to a locally occurring anharmonic motion of the tip[33,34] at these small tip-sample distances. The two-dimensional histogram of the pixelwise correlation of I_2 and A_2 (Figure 4d) confirms this interpretation, showing that for A_2 values over 4 pm I_2 seems to be increasing with A_2 — a relation discernible only thanks to the remarkable stability and sensitivity of our probe.

Quantitatively, the linear correlation can be described by the Pearson correlation coefficient r, which ranges from −1 (perfect negative linear correlation) to +1 (perfect positive linear correlation), with r = 0 indicating no linear relationship.[35] For this data set, we obtain r = 0.305, indicating a weak to moderate positive correlation. This is a crucial insight showing that for all measurements performed with similar setups in the future, measuring the harmonicity of the tip oscillation is imperative for reliable results at such small tip-sample distances. Since for A_2 < 4 pm no obvious correlation between A_2 and I_2 can be observed, we define a threshold and exclude all data points with second harmonic amplitude contributions of A_2 > 4 pm (marked regions in Figure 4b,c and to the right of the dashed line in Figure 4d). Reassessing the correlation between I_2 and A_2 using only the remaining 86% of data, we obtain a Pearson coefficient of r = 0.096, hinting toward no pronounced linear correlation.[35] This indicates that, despite the localized enhancement of A_2, the optical signal I_2 remains unaffected across the vast majority of locations. Notably, applying the same thresholding procedure to the scan

https://doi.org/10.1021/acs.nanolett.5c05319
Nano Lett. 2026, 26, 1689−1696

shown in Figure 3 would result in the exclusion of only 10 data points, retaining 99.6% of the scan (Supporting Information Section 10). To exclude the possibility that variations in A_2 account for the observed optical behavior in Figure 1, we performed an analogous measurement while tracking A_2, which yields qualitatively similar optical signals while A_2 remains flat (Supporting Information Section 11).

Thus, one can reliably extract the local optical response by carefully monitoring the tip oscillation and only evaluating regions where the local amplitude A_2 remains well-behaved. Alternatively, anharmonic tip motion can be effectively suppressed by choosing a suitable tip-sample distance, balancing signal strength and well-behaved tip motion. To this end, we investigate the dependence of I_2 and A_2 on the tip-sample distance z at one position in detail (Figure 4e). I_2 increases exponentially with a nonzero signal already present at the highest tip-sample distance of 300 pm and a 1/e decay length of 77 pm. The simultaneously recorded data for A_2 show a similar behavior, however, first remaining below the noise threshold (~4 pm) for larger separations and only exponentially increasing at distances below ~120 pm with a 1/e value of 40 pm. Hence there is a finite tuning range of tip-sample distances where I_2 is already nonzero while A_2 remains negligible, thus establishing a practical regime where tunneling-current-mediated optical contrast can be accessed even with standard tabletop continuous-wave laser sources.

In conclusion, we combined an ultrahigh-vacuum scanning probe microscope capable of picometric tip control with a standard optical setup for near-field microscopy using a commercial quantum cascade laser and pseudoheterodyne photodiode detection. At atomic-scale tip-sample distances, we observed a signal exhibiting the two hallmark features of NOTE: a picometric vertical decay and a distinct phase shift relative to the conventional near-field response — both consistent with our TDM. We achieved atomic-scale optical microscopy on a vicinal gold surface, where the scattered intensity showed a clear positive correlation with the tunneling current, in line with the NOTE mechanism. At extremely small tip-sample distances, a second harmonic contribution in the tip's oscillation emerges — an effect that can potentially give rise to artifactual signals. By closely monitoring the tip's mechanical behavior, we identified a stable operational regime in which the tunneling-related contrast mechanism can be reliably used to extract signal modulations on the Ångstrom length scale with artifacts from anharmonic tip oscillation effectively ruled out.

Our findings represent an important step toward the broader adoption of atomic-scale optical microscopy, combining the spatial resolution of scanning probe techniques such as STM and AFM with the frequency selectivity of near-field microscopy. This opens the door to extend the toolbox of atomic-scale spectroscopy: By tuning the optical frequency, one could map the local dielectric function, while sweeping the tip-sample bias may allow the optical signal to probe differential conductance in this highly nonequilibrium state. As NOTE does not rely on a net current to flow, it is compatible even with insulating samples, where this concept could be particularly intriguing: The sensitivity to all tunneling carriers — not only those that are rectified — could enable the investigation of tunneling processes that remain hidden to conventional electronic detection. More broadly, our results contribute to a deeper understanding of atomic-scale interactions in tip-based optical measurements — a key to advancing nanoscale spectroscopy and imaging.

■ ASSOCIATED CONTENT

Data Availability Statement

The data sets generated during and/or analyzed during the current study are available from the corresponding author upon request.

Supporting Information

The Supporting Information is available free of charge at https://pubs.acs.org/doi/10.1021/acs.nanolett.5c05319.

(1) Low-temperature near-field microscopy setup; (2) Optical setup for mid-infrared NOTE microscopy; (3) Details on the tips used in the experiment; (4) Calibration of the absolute tip-sample distance; (5) Details of the tunneling dipole model; (6) Estimation of the lightwave-induced bias under cw illumination; (7) Background-free near-field detection at small oscillation amplitudes; (8) Statistical analysis of the modulation length of the NOTE signal; (9) Calibration of the tip oscillation amplitude; (10) Excluding anharmonicity artifacts in the 2D scan of Figure 3; (11) Excluding anharmonicity artifacts as the origin of the optical signals in Figure 1 (PDF)

■ AUTHOR INFORMATION

Corresponding Authors

Markus A. Huber − *Department of Physics and Regensburg Center for Ultrafast Nanoscopy (RUN), University of Regensburg, 93040 Regensburg, Germany;* orcid.org/0000-0001-5324-9895; Email: markus.huber@ur.de

Thomas Siday − *School of Physics and Astronomy, University of Birmingham, Birmingham B15 2TT, U.K.;* orcid.org/0000-0003-0157-3233; Email: t.siday@bham.ac.uk

Authors

Felix Schiegl − *Department of Physics and Regensburg Center for Ultrafast Nanoscopy (RUN), University of Regensburg, 93040 Regensburg, Germany;* orcid.org/0009-0002-2963-4130

Valentin Bergbauer − *Department of Physics and Regensburg Center for Ultrafast Nanoscopy (RUN), University of Regensburg, 93040 Regensburg, Germany*

Svenja Nerreter − *Department of Physics and Regensburg Center for Ultrafast Nanoscopy (RUN), University of Regensburg, 93040 Regensburg, Germany*

Valentin Giessibl − *Department of Physics and Regensburg Center for Ultrafast Nanoscopy (RUN), University of Regensburg, 93040 Regensburg, Germany*

Fabian Sandner − *Department of Physics and Regensburg Center for Ultrafast Nanoscopy (RUN), University of Regensburg, 93040 Regensburg, Germany*

Franz J. Giessibl − *Department of Physics and Regensburg Center for Ultrafast Nanoscopy (RUN), University of Regensburg, 93040 Regensburg, Germany;* orcid.org/0000-0002-5585-1326

Yaroslav. A. Gerasimenko − *Department of Physics and Regensburg Center for Ultrafast Nanoscopy (RUN), University of Regensburg, 93040 Regensburg, Germany*

https://doi.org/10.1021/acs.nanolett.5c05319
Nano Lett. 2026, 26, 1689−1696

Rupert Huber − *Department of Physics and Regensburg Center for Ultrafast Nanoscopy (RUN), University of Regensburg, 93040 Regensburg, Germany*

Complete contact information is available at: https://pubs.acs.org/10.1021/acs.nanolett.5c05319

Author Contributions

#F. Schiegl and V.B. contributed equally. T.S., M.A.H., and R.H. conceived the study. F. Schiegl, V.B., S.N., V.G., F. Sandner, Y.A.G., T.S., and M.A.H. performed the experiments and analyzed the data. F. Schiegl, V.B., S.N., V.G., F. Sandner, Y.A.G., and T.S. fabricated the samples. F. Schiegl, V.B., S.N., V.G., F. Sandner, F.J.G., Y.A.G., T.S., M.A.H., and R.H. contributed to the discussions of the experimental results. F. Schiegl, V.B., S.N., V.G., T.S., and M.A.H. computed the tunneling dipole model. The manuscript was written by F. Schiegl, V.B., S.N., T.S., M.A.H., and R.H. with input and contributions from all authors. All authors have given approval to the final version of the manuscript.

Funding

This work was supported by the Deutsche Forschungsgemeinschaft (DFG, German Research Foundation) through SFB 1277 − project-ID 314695032, GRK 2905 − project-ID 502572516, major instrumentation grant INST 89/505−1 FUGG − project-ID 417226546, and through research grant HU1598/8-1.

Notes

The authors declare the following competing financial interest(s): The University of Regensburg applied for a German patent (DE 10 2024 108 203 A1) as well as a European patent (no. 25 163 001.8) on near-field optical tunnelling emission microscopy. The authors declare no further competing interests.

■ ACKNOWLEDGMENTS

We thank Franco Bonafé, Angel Rubio, and Jan Wilhelm for helpful discussions and Martin Furthmeier and Matthias Heinl for technical assistance.

■ REFERENCES

(1) Hell, S. W. Far-Field Optical Nanoscopy. *Science* **2007**, *316*, 1153−1158.
(2) Baumberg, J. J. Picocavities: a Primer. *Nano Lett.* **2022**, *22*, 5859−5865.
(3) Novotny, L.; Hecht, B. *Principles of Nano-Optics*, 2nd ed.; Cambridge University Press: 2012.
(4) Hillenbrand, R.; Abate, Y.; Liu, M.; Chen, X.; Basov, D. N. Visible-to-THz near-field nanoscopy. *Nature Reviews Materials* **2025**, *10*, 285−310.
(5) Taubner, T.; Hillenbrand, R.; Keilmann, F. Performance of visible and mid-infrared scattering-type near-field optical microscopes. *J. Microsc.* **2003**, *210*, 311−314.
(6) Fei, Z.; Rodin, A. S.; Andreev, G. O.; Bao, W.; McLeod, A. S.; Wagner, M.; Zhang, L. M.; Zhao, Z.; Thiemens, M.; Dominguez, G.; Fogler, M. M.; Neto, A. H. C.; Lau, C. N.; Keilmann, F.; Basov, D. N. Gate-tuning of graphene plasmons revealed by infrared nano-imaging. *Nature* **2012**, *487*, 82−85.
(7) Chen, J.; Badioli, M.; Alonso-González, P.; Thongrattanasiri, S.; Huth, F.; Osmond, J.; Spasenović, M.; Centeno, A.; Pesquera, A.; Godignon, P.; Zurutuza Elorza, A.; de Camara, N.; García, F. J.; Hillenbrand, R.; Koppens, F. H. Optical nano-imaging of gate-tunable graphene plasmons. *Nature* **2012**, *487*, 77−81.
(8) Eisele, M.; Cocker, T. L.; Huber, M. A.; Plankl, M.; Viti, L.; Ercolani, D.; Sorba, L.; Vitiello, M. S.; Huber, R. Ultrafast multi-terahertz nanospectroscopy with sub-cycle temporal resolution. *Nat. Photonics* **2014**, *8*, 841−845.
(9) Huber, M. A.; Mooshammer, F.; Plankl, M.; Viti, L.; Sandner, F.; Kastner, L. Z.; Frank, T.; Fabian, J.; Vitiello, M. S.; Cocker, T. L.; Huber, R. Femtosecond photo-switching of interface polaritons in black phosphorus heterostructures. *Nat. Nanotechnol.* **2017**, *12*, 207−211.
(10) Zhang, Q.; Hu, G.; Ma, W.; Li, P.; Krasnok, A.; Hillenbrand, R.; Alù, A.; Qiu, C. W. Interface nano-optics with van der Waals polaritons. *Nature* **2021**, *597*, 187−195.
(11) Siday, T.; Sandner, F.; Brem, S.; Zizlsperger, M.; Perea-Causin, R.; Schiegl, F.; Nerreter, S.; Plankl, M.; Merkl, P.; Mooshammer, F.; Huber, M. A.; Malic, E.; Huber, R. Ultrafast Nanoscopy of High-Density Exciton Phases in WSe2. *Nano Lett.* **2022**, *22*, 2561−2568.
(12) Kim, R. H. J.; Park, J.-M.; Haeuser, S. J.; Luo, L.; Wang, J. A sub-2 K cryogenic magneto-terahertz scattering-type scanning near-field optical microscope (cm-THz-sSNOM). *Rev. Sci. Instrum.* **2023**, *94*, 043702.
(13) Zizlsperger, M.; Nerreter, S.; Yuan, Q.; Lohmann, K. B.; Sandner, F.; Schiegl, F.; Meineke, C.; Gerasimenko, Y. A.; Herz, L. M.; Siday, T.; Huber, M. A.; Johnston, M. B.; Huber, R. In situ nanoscopy of single-grain nanomorphology and ultrafast carrier dynamics in metal halide perovskites. *Nat. Photonics* **2024**, *18*, 975−981.
(14) Anglhuber, S.; Zizlsperger, M.; Pogna, E. A.; Gerasimenko, Y. A.; Koulouklidis, A. D.; Gronwald, I.; Nerreter, S.; Viti, L.; Vitiello, M. S.; Huber, R.; Huber, M. A. Spacetime Imaging of Group and Phase Velocities of Terahertz Surface Plasmon Polaritons in Graphene. *Nano Lett.* **2025**, *25*, 2125−2132.
(15) Giessibl, F. J. Advances in atomic force microscopy. *Rev. Mod. Phys.* **2003**, *75*, 949−983.
(16) Shiotari, A.; Nishida, J.; Hammud, A.; Schulz, F.; Wolf, M.; Kumagai, T.; Müller, M. Scattering near-field optical microscopy at 1-nm resolution using ultralow tip oscillation amplitudes. *Science Advances* **2025**, *11*, No. eadu1415.
(17) Cocker, T. L.; Peller, D.; Yu, P.; Repp, J.; Huber, R. Tracking the ultrafast motion of a single molecule by femtosecond orbital imaging. *Nature* **2016**, *539*, 263−267.
(18) Peller, D.; Kastner, L. Z.; Buchner, T.; Roelcke, C.; Albrecht, F.; Moll, N.; Huber, R.; Repp, J. Sub-cycle atomic-scale forces coherently control a single-molecule switch. *Nature* **2020**, *585*, 58−62.
(19) Jelic, V.; Adams, S.; Hassan, M.; Cleland-Host, K.; Ammerman, S. E.; Cocker, T. L. Atomic-scale terahertz time-domain spectroscopy. *Nat. Photonics* **2024**, *18*, 898−904.
(20) Roelcke, C.; Kastner, L. Z.; Graml, M.; Biereder, A.; Wilhelm, J.; Repp, J.; Huber, R.; Gerasimenko, Y. A. Ultrafast atomic-scale scanning tunnelling spectroscopy of a single vacancy in a monolayer crystal. *Nat. Photonics* **2024**, *18*, 595−602.
(21) Siday, T.; Hayes, J.; Schiegl, F.; Sandner, F.; Menden, P.; Bergbauer, V.; Zizlsperger, M.; Nerreter, S.; Lingl, S.; Repp, J.; Wilhelm, J.; Huber, M. A.; Gerasimenko, Y. A.; Huber, R. All-optical subcycle microscopy on atomic length scales. *Nature* **2024**, *629*, 329−334.
(22) Borsch, M.; Meierhofer, M.; Huber, R.; Kira, M. Lightwave electronics in condensed matter. *Nature Review Materials* **2023**, *8*, 668−687.
(23) Zaks, B.; Liu, R. B.; Sherwin, M. S. Experimental observation of electron-hole recollisions. *Nature* **2012**, *483*, 580−583.
(24) Ocelic, N.; Huber, A.; Hillenbrand, R. Pseudoheterodyne detection for background-free near-field spectroscopy. *Appl. Phys. Lett.* **2006**, *89*, 101124.
(25) Gimzewski, J. K.; Möller, R. Transition from the tunneling regime to point contact studied using scanning tunneling microscopy. *Phys. Rev. B* **1987**, *36*, 1284−1287.
(26) Knoll, B.; Keilmann, F. Near-field probing of vibrational absorption for chemical microscopy. *Nature* **1999**, *399*, 134−137.

(27) Babushkin, I.; Galán, Á. J.; de Andrade, J. R. C.; Husakou, A.; Morales, F.; Kretschmar, M.; Nagy, T.; Vaičaitis, V.; Shi, L.; Zuber, D.; Bergé, L.; Skupin, S.; Nikolaeva, I. A.; Panov, N. A.; Shipilo, D. E.; Kosareva, O. G.; Pfeiffer, A. N.; Demircan, A.; Vrakking, M. J. J.; Morgner, U.; Ivanov, M. All-optical attoclock for imaging tunnelling wavepackets. *Nat. Phys.* **2022**, *18*, 417−422.
(28) Keldysh, L. V. Ionization in the Field of a Strong Electromagnetic Wave. *Soviet Physics JETP* **1965**, *20*, 1307−1314.
(29) Chen, C. J. Introduction to Scanning Tunneling Microscopy, 2nd ed.; Oxford University Press: Oxford, 2008.
(30) Yang, H. U.; Hebestreit, E.; Josberger, E. E.; Raschke, M. B. A cryogenic scattering-type near-field optical microscope. *Rev. Sci. Instrum.* **2013**, *84*, 023701.
(31) Mugarza, A.; Ortega, J. E. Electronic states at vicinal surfaces. *J. Phys.: Condens. Matter* **2003**, *15*, S3281−S3310.
(32) Ortega, J. E.; Mugarza, A.; Schiller, F.; Lobo-Checa, J.; Corso, M. *Electronic States of Vicinal Surfaces*; Springer: Cham, 2020; pp 351−385.
(33) Hembacher, S.; Giessibl, F. J.; Mannhart, J. Force microscopy with light-atom probes. *Science* **2004**, *305*, 380−383.
(34) Giessibl, F. J. Higher-harmonic atomic force microscopy. *Surf. Interface Anal.* **2006**, *38*, 1696−1701.
(35) Kuckartz, U.; Rädiker, S.; Ebert, T.; Schehl, J. *Statistik*; VS Verlag für Sozialwissenschaften: Wiesbaden, 2013.

https://doi.org/10.1021/acs.nanolett.5c05319
Nano Lett. 2026, 26, 1689−1696